Development of an N-body interatomic potential for hcp and bcc zirconium

F. Willaime
Centre d'Etudes de Saclay, Section de Recherches de Métallurgie Physique, 91191 Gif-sur-Yvette CEDEX, France

C. Massobrio
Laboratoire des Composés Non-Stoechiométriques, Université de Paris–Sud, 91405 Orsay CEDEX, France

(Received 12 November 1990)

An interatomic potential based on the second-moment approximation of the tight-binding scheme is developed for zirconium, by fitting its four adjustable parameters to the cohesive energy, atomic volume, and elastic constants of the hcp phase. In this work we attempt to model realistically two different crystallographic phases of a solid with the same potential. The reliability of our potential is tested in both the hcp and the bcc phases with regard to defect properties, thermal expansion, phonon properties, and mean-square displacements. For this purpose, we perform quenched molecular-dynamics relaxations, quasiharmonic lattice-dynamics calculations, and molecular-dynamics simulations. The low vacancy-formation and migration energies found in the bcc phase are consistent with the fast diffusivity experimentally observed. Unlike some other N-body potentials recently proposed to model bcc transition metals, our potential is not affected by the flaw of unphysical or even negative thermal expansion. We obtain thermal expansions that agree well with experiments in both phases, although they turned out to be slightly too large. The phonon-dispersion curves and, in particular, the anomalies in the bcc phase are well reproduced. We emphasize the stabilization with temperature of the $T1$ N-point phonon of the bcc phase, which is related to the bcc- to hcp-phase transition. We obtain a temperature dependence of this mode much weaker than in the experimental case. This influences the temperature behavior of the vibrational properties: In particular the mean-square displacement is markedly higher than the one extracted from experiments in the bcc phase at high temperatures. On the other hand, mean-square displacements in the hcp phase are in excellent agreement with experiment. The results are quite satisfactory in view of the small number of fitting parameters and the difficulties commonly encountered in matching the properties of bcc metals.

I. INTRODUCTION

The development of many-body potentials witnessed in recent years represents a major improvement in the domain of atomic-scale calculations. In particular, for transition metals, potentials based on the embedded-atom method (EAM) of Daw and Baskes,[1] the Finnis-Sinclair[2] (FS) scheme, and the Rosato-Guillopé-Legrand[3] (RGL) scheme have been devised to model the metallic cohesion and account realistically for a large variety of properties treated inadequately by simple pair potentials. We recall that pair potentials lead to a vacancy-formation energy about equal to the cohesive energy and cannot describe the elastic properties of metals since they yield a vanishing Cauchy discrepancy, $C_{12}=C_{44}$. N-body potentials have been implemented to cope with these limitations. In the EAM case, the energy of the system is viewed as the energy required to embed a given atom into the local electron density provided by the remaining atoms plus a core-core repulsion potential which takes the form of a pair potential. The potential energy is written as

$$E_{\rm pot}=\sum_i F_i(\rho i)+\sum_i \sum_{j\,(\neq i)} \Phi(r_{ij}) \ , \tag{1}$$

$$E_{\rm pot}=\sum_i F_i\left[\sum_{j\,(\neq i)} \rho_j^a(r_{ij})\right]+\sum_i \sum_{j\,(\neq i)} \Phi(r_{ij}) \ . \tag{2}$$

F_i is called the embedding energy of atom i, ρ_i is the electron density at atom i, and $\Phi(r_{ij})$ the repulsive interaction between pairs of atoms separated by a distance r_{ij}. Equation (2) is obtained from (1) by approximating the electron densities ρ_i pertaining to each atom in (1) with the superposition of the atomic electron densities ρ_j^a from the other atoms. Physical motivations for the EAM as well as practical details of the empirical fitting leading to a complete determination of the embedding energies and pairs interactions have been documented elsewhere.[1,4]

We point out that a derivation of the EAM formalism from first principles has been recently worked out.[5] An analytical form closely similar to the one given in (1) but based on a somewhat different physical interpretation has been proposed first by Finnis and Sinclair[2] and later by Rosato, Guillopé, and Legrand[3] with the intent of performing large-scale atomistic computations [Monte Carlo (MC) and molecular-dynamics (MD) simulations]. Their approach is related to the second-moment approximation of the tight-binding electronic density of states and follows the line pioneered by Friedel[6] and Ducastelle.[7]

Within this approximation, the energy of the d band is proportional to the square root of the second moment of the density of states. The latter is expressed in terms of a sum of the square of the hopping or transfer integrals and accordingly the potential energy takes the form

$$E_{\rm pot} = -\sum_i \left[\sum_{j\,(\neq i)} f^2(r_{ij}) \right]^{1/2} + \sum_i \sum_{j\,(\neq i)} \Phi(r_{ij}) \ , \qquad (3)$$

where $f(r_{ij})$ is proportional to the transfer integral between atoms i and j separated by the distance r_{ij} and the repulsive pair potential Φ is once again required to guarantee the stability of the lattice. The RGL and FS approaches differ in the form of the f and Φ functions: They are taken to be exponentials in the first case (as suggested by Friedel and Ducastelle) and polynomials in the second. In practical applications, the range of the interactions and the potential parameters are determined by computational convenience and empirical fitting.[2,3,8,9]

A remarkable feature common to the three families of potentials outlined above is the introduction of the N-body character through the functional appearing in the attractive term (square root for the tight-binding-related expressions, and F_i to be fitted in the EAM case). EAM and RGL potentials have been successfully employed to calculate static and thermodynamical bulk,[4,10] surface,[4,8,11,12] and defect[3,13] properties of fcc metals. In particular, thermal expansions calculated for a set of EAM fcc potentials[14] and for Cu (Ref. 12) in the RGL case as well as phonon dispersions[3,15] were found to be in good agreement with experiment. Applications of N-body potentials to hcp metals are rather scarce and to our knowledge limited to the work by Oh and Johnson[16] within the EAM scheme and by Igarashi *et al.*[17] using FS potentials. More problems were encountered for bcc transition metals. Despite the modifications to the original FS potentials introduced by Rebonato *et al.*[9] and by Ackland and Thetford[18] improving the pressure-versus-volume relations, thermal expansions are modeled inaccurately by most FS potentials constructed for bcc metals.[19] As to phonon properties, the agreement with experiments for the dispersion curves calculated by using FS potentials[20] was found to be satisfactory for Mo and W but poor for Ta, V, and Nb. For this last metal, Eridon and Rao[21] were able to achieve a good fitting to the experimental data "but the predictive capabilities of this model away from the region of the configurational space in which it was constructed has not been tested." More promising in this direction appears to be the EAM approach as shown recently by Adams and Foiles that implemented a highly satisfactory potential for vanadium[22] to study bulk and defects properties of this metal. On the other hand, no attention has been paid so far to the high-temperature bcc phase of the elements of group IVa (Ti, Zr, and Hf) that have the feature of undergoing a bcc- to hcp-phase transformation when lowering the temperature. Given the intriguing and still unexplained peculiarities of high-temperature diffusion in these metals[23] it would be desirable to rely on an appropriate description at the atomistic level of their bcc phases. Moreover, we are unaware of any attempts to achieve a realistic modeling of different crystallographic phases of the same element by employing the same N-body interatomic potential. The main purpose of this work is to present the development of an interatomic potential for Zr that meets these requirements.

As shown in a preliminary report,[24] the potential that we constructed in the framework of the RGL scheme is well behaved when tested against elastic and phonon properties of both hcp and bcc phases and accounts properly for the stabilization of the bcc phase at high temperatures. This paper details the implementation and the assessment of the reliability of the potential with respect to defect properties, phonon-dispersion curves, and dynamical behavior. For this purpose, we performed quasiharmonic lattice-dynamics computations and molecular-dynamics simulations. A forthcoming paper will be devoted entirely to the mechanisms and the energetics of the hcp-bcc phase transition.[25] The paper is organized as follows. In Sec. II we describe the implementation and the practical layout of the fitting procedure and we place special emphasis on the cutoff-radius dependence of the stability of a given phase. We compare also the elastic properties of the static lattice in the hcp and bcc phases to experimental results. In Sec. III we describe the computational techniques. Section IV is devoted to a presentation of the results for defect properties, thermal expansion, phonon properties (highlighting, in particular, the temperature dependence of the T1 N-point mode), the mean-square displacements. Conclusions are drawn in Sec. V.

II. THE MODEL

A. Interatomic potential for Zr

The potential we use has the analytical form introduced in the original paper of RGL,[3] namely, the total potential energy of an assembly of N atoms is

$$E_{\rm pot} = \sum_{i=1}^{N} E_i \ , \qquad (4)$$

where E_i, the contribution of atom i, is the sum of two terms:

$$E_i = E_i^r + E_i^b \ , \qquad (5)$$

$$E_i^r = \sum_{j\,(\neq i)} \Phi(r_{ij}) = A \sum_{j\,(\neq i)} \exp\left\{ -\left[p\left[\frac{r_{ij}}{r_0} - 1 \right] \right] \right\} \ , \qquad (6)$$

$$E_i^b = -\left\{ \sum_{j\,(\neq i)} f^2(r_{ij}) \right\}^{1/2} = -\left\{ \sum_{j\,(\neq i)} \exp\left\{ -\left[2q\left[\frac{r_{ij}}{r_0} - 1 \right] \right] \right\} \right\}^{1/2} \ , \qquad (7)$$

where A, ξ, p, and q are the four adjustable parameters of the potential. E_i^r is a repulsive pairwise interaction of the Born-Mayer type and E_i^b is the tight-binding d-band energy for transition metals approximated by its second moment. The interactions in (6) and (7) are calculated up to a distance $r_{\rm cut}$, whereas r_0 is taken to be the nearest-

neighbor distance; p and q are thus dimensionless. Note that r_0 is not an additional fitting parameter. We fixed the value of r_0 by extrapolation to zero temperature of the experimental value of the nearest-neighbor distance in the hcp phase of zirconium ($r_0=0.31744$ nm). It is worth commenting at this stage on the suitability of the second-moment approximation in the form given by (6) and (7) to describe correctly the cohesion in transition metals for different crystalline structures. For closed-packed phases (hcp or fcc), the second-moment approximation gives an excellent representation of elastic properties.[3,7] On the other hand, the second-moment approximation in the RGL form is commonly unfit to reproduce the shear anisotropy ratio C_{44}/C' of bcc metals. With interactions restricted to nearest neighbors, C' is equal to zero for the equilibrium structure, regardless of the analytical form of the f and Φ functions in (6) and (7). By accounting for next-neighbor interactions and keeping the same cutoff radius for both attractive and repulsive contributions, we found empirically the following behavior: Whenever we tried to fit the potential to the cohesive energy, the lattice parameter and the elastic constants of any bcc metal, we obtained a value for C' between -0.1×10^{12} and 0.1×10^{12} dyn/cm^2. Consequently, the form of the potential that we adopted does not allow one to match the much larger C' (from 0.5×10^{12} up to 1.6×10^{12} dyn/cm^2)[26] typical of the elements of columns V and VI (V, Nb, Ta, Cr, Mo, and W). Conversely, metals of column IV, such as zirconium, characterized by a relatively small C' (0.06×10^{12} dyn/cm^2) (Ref. 27) are likely to be described more adequately. This stumbling block regarding the C' behavior displayed by potential models for bcc metals has been noted also by Oh and Johnson[16] using the EAM approach. In this context, we draw attention on a recent numerical work performed by Legrand[28] that obtained a good agreement with experimental results for the variation of C' as a function of the filling of the d band. Legrand made use of a tight-binding expansion of the energy up to the fifth moment of the density of states (the result remains unchanged while going up to the nineteenth moment). Elastic constants of Fe, Nb, Mo, and W were also successfully calculated by Masuda *et al.* using a tight-binding recursion method.[29]

B. Fitting procedure

The parameters A, ξ, p, and q in (6) and (7) are fitted to static properties of hcp zirconium at zero temperature. We performed a series of fits for different cutoff radii $r_{\rm cut}$. For a given $r_{\rm cut}$, we fitted A, ξ, p, and q to the cohesive energy, the atomic volume, and the elastic constants as follows: The cohesive energy of our model is required to be equal to the experimental value E_c and, therefore

$$AS_1-\xi\sqrt{S_2}=-E_c\ , \tag{8}$$

where

$$S_1=\sum_{j\,(\neq i)}\exp\left\{-\left[p\left[\frac{r_{ij}}{r_0}-1\right]\right]\right\} \tag{9}$$

and

$$S_2=\sum_{j\,(\neq i)}\exp\left\{-\left[2q\left[\frac{r_{ij}}{r_0}-1\right]\right]\right\}. \tag{10}$$

The summations include all neighbors j of a given atom i for which $r_{ij}<r_{\rm cut}$. The condition of zero pressure implies that

$$AS_1'-\xi\frac{S_2'}{\sqrt{S_2}}=0\ , \tag{11}$$

where

$$S_1'=\sum_{j(\neq i)}pr_{ij}\exp\left\{-\left[p\left[\frac{r_{ij}}{r_0}-1\right]\right]\right\} \tag{12}$$

and

$$S_2'=\sum_{j(\neq i)}qr_{ij}\exp\left\{-\left[2q\left[\frac{r_{ij}}{r_0}-1\right]\right]\right\}. \tag{13}$$

Equations (8) and (11) can be rewritten as follows:

$$A=\frac{E_cS_2'}{S_2S_1'-S_1S_2'}\ , \tag{14}$$

$$\xi=\frac{E_cS_1'\sqrt{S_2}}{S_2S_1'-S_1S_2'}\ . \tag{15}$$

This means that for a given choice of the lattice constants a and c and of the parameters p and q the values of A and ξ leading to the experimental cohesive energy and zero pressure are given in (14) and (15). The equilibrium atomic volume is set equal to the experimental volume Ω_0, namely, the lattice parameters $a_{\rm eq}$ and $c_{\rm eq}$ corresponding to zero stress-tensor components σ_{ij} are such that

$$a_{\rm eq}^2c_{\rm eq}\sqrt{3}/4=\Omega_0\ . \tag{16}$$

In a noncubic structure, Eq. (11) does not necessarily imply that $\sigma_{ij}=0$. To satisfy this condition, we proceed in two independent steps. First we set the c/a ratio equal to the ideal value $\sqrt{8/3}$, a and c being calculated from (16). Then p and q are determined by minimizing the difference between experimental and calculated elastic constants. We performed a minimization involving all elastic constants, rather than choosing some of them and obtaining poor agreement for the others. With these values of p and q, we then by trial and error looked for the c/a ratio leading to $\sigma_{ij}=0$: We chose a value for c/a, recalculate A and ξ by (14) and (15) until $|\sigma_{ij}|<0.05$ kbar. The best fit was obtained by setting $p=9.3$ and $q=2.1$ throughout the fitting procedure. The cohesive energy is then calculated for the fcc and bcc structures with their lattice parameters corresponding to zero pressure.

As shown in Fig. 1, the stable phase is alternatively hcp, bcc, or fcc for different values of $r_{\rm cut}$. For small $r_{\rm cut}$, the stable phase is generally the one which has the largest number of interacting neighbors per atom. For larger $r_{\rm cut}$, the potential stabilizes the hcp structure. The cohesive energies of the fcc and hcp phases are very close to each other as observed in the case of the Lennard

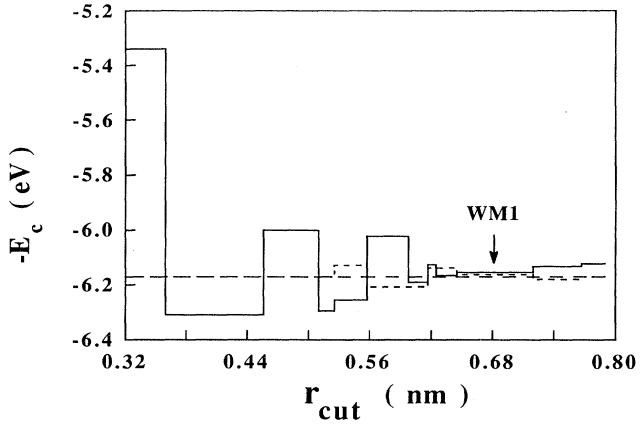

FIG. 1. Cohesive energy in various crystal structures, hcp (long dashed), fcc (short dashed), and bcc (solid) as a function of the cutoff radius for the RGL potential fitted to hcp Zr. A fit is made for every additional neighbor shell of the hcp structure. The fitting procedure requires the cohesive energy in the hcp phase to be equal to its experimental value, i.e., 6.17 eV.

TABLE I. Parameters of our potentials for Zr for two different cutoff radii. The properties of the hcp phase used for the fit are the cohesive energy, E_c, the atomic volume, Ω_0, and the elastic constants, C_{ij}. A, ξ, and E_c are expressed in eV per atom, the distances in nm, Ω_0 in $\mathrm{cm^3\,mol^{-1}}$, and C_{ij} in 10^{12} $\mathrm{dyn\,cm^{-2}}$.

	$WM2$	$WM1$	Experiments
r_{cut}	0.54	0.68	
r_0	0.31744	0.317 44	
p	9.3	9.3	
q	2.1	2.1	
A	0.167 02	0.179 364	
ξ	2.254 948	2.201 42	
a	0.321 96	0.320 2	0.322 61[a]
c/a	1.603 25	1.629 8	1.595[a]
E_c	6.17	6.17	6.17[a]
Ω_0	13.95	13.95	13.95[a]
C_{11}	1.54	1.62	1.554[b]
C_{12}	0.70	0.77	0.672 3[b]
C_{13}	0.65	0.65	0.646[b]
C_{44}	0.34	0.30	0.363[b]
B	0.97	1.01	0.9734[b]

[a]Reference 31.
[b]Reference 27.

Jones potential which stabilizes either one of the two phases, depending on the cutoff radius.[30] In Zr the hcp phase is stable at zero temperature but the energy difference with the bcc phase is quite small. To reproduce this feature and obtain the largest cohesive energy in the hcp structure, we choose $r_{\mathrm{cut}}=0.68$ nm (see Fig. 1). Hereafter the potential resulting from the fit performed with this value of r_{cut} will be denoted $WM1$. The total number of neighbor shells is six in the hcp phase and five in the bcc phase, leading to 56 and 58 interactions per atom, respectively. As we shall see in Sec. IV some phonon frequencies in the bcc structure are imaginary within the quasiharmonic approximation for this potential. Therefore a different potential stabilizing the bcc structure is needed to perform quasiharmonic calculations involving sums over phonon modes. For this purpose, we employed a potential (hereafter denoted $WM2$) issued from the fit with $r_{\mathrm{cut}}=0.54$ nm and characterized by positive phonon frequencies and largest cohesive energy in the bcc phase with respect to the hcp and fcc phases. The parameters of the potentials $WM1$ and $WM2$, as well as the comparison between the experimental and calculated values of physical quantities entering the fit, are summarized in Table I.

A comment is in order on some outcomes of the fitting procedure. First, we notice, from Table I, that the experimental value of the c/a ratio $[(c/a)^{\mathrm{expt}}=1.595]$ is slightly smaller than the ideal value $[(c/a)^{\mathrm{ideal}}=\sqrt{8/3}=1.633]$ for the hexagonal structure. Ducastelle[32] demonstrated that the second-moment approximation with interactions restricted to nearest neighbors yields the same cohesive energy for the hcp and the fcc phases and a c/a ratio equal to the ideal value. The fourth-moment approximation is required to make a difference between fcc and the hcp and to give values of c/a other than $\sqrt{8/3}$. That $c/a\neq(c/a)^{\mathrm{ideal}}$ in our models is therefore due to the extension of the interactions to further neighbors. Furthermore, we observe that the agreement between experimental and calculated values of elastic constants is more satisfactory in the case of the WM2 potential and, in particular, for the elastic constant C_{44}. This pecularity has to be related to the value of the c/a ratio which is closer to the experimental one. Indeed, we obtain a much better agreement for C_{44} by employing the $WM1$ potential on a nonequilibrium structure by imposing a c/a ratio equal to $(c/a)^{\mathrm{expt}}$. We mention that Igarashi *et al.*,[17] in their application of FS potentials on hcp metals, were able to reproduce the experimental c/a ratio. This has been made possible by writing the f and Φ functions in Eq. (3) as sums of interactions of different range, but this strategy required up to ten adjustable parameters.

C. Static properties of the bcc phase

It is of some interest to compare static properties of the bcc phase of our $WM1$ potential with experimental values at temperatures larger than the hcp-bcc experimental transition temperature ($T^{\mathrm{tr}}=1136$ K) or extrapolated therefrom. As expected, given the choice of the cutoff radius, the enthalpy difference between the bcc and the hcp phase, $H_{\mathrm{bcc}}-H_{\mathrm{hcp}}=0.027$ eV, is positive and remarkably close to the experimental value at T^{tr}. Table II contains elastic-constant calculations on the static lattice and their experimental counterpart at $T=1188$ K. We find reasonable agreement for C_{11} and C_{12}, but an unsatisfactory one for C_{44}. It is instructive to compare the shear moduli C' relative to the instability of the bcc phase and the mechanism of the phase transformation. In the experimental case, C' is equal to 6×10^{10} dyn/cm^2, the calculated C' being equal to 7×10^{9} dyn/cm^2. The

TABLE II. Characteristics of the $WM1$ potential in the bcc phase at zero pressure compared with experiments. The energy are expressed in eV per atom, the elastic constants in 10^{12} dyn cm^2, and the lattice parameters in nm.

	$WM1$	Experiments
$H_{bcc}-H_{hcp}$	0.03[a]	0.04[b]
C_{11}	1.011[a]	1.04[c]
C_{12}	0.997[a]	0.93[c]
C_{44}	0.656[a]	0.38[c]
B	1.002[a]	0.97[c]
a	0.3595[a]	0.3574[d]

[a]Static calculations.
[b]Experimental value at 1135 K (Ref. 31).
[c]Experimental value at 1188 K (Ref. 27).
[d]Extrapolation at 0 K of the linear fit on the experimental values of Ref. 27 in the range 1200 to 1600 K.

agreement is favorable, both values being quite small compared with C' for bcc metals of columns Va and VIa ($0.5\times10^{12}<C'<1.6\times10^{12}$ dyn/cm^2).[26]

III. CALCULATIONAL TECHNIQUES

A. Molecular-dynamics simulations

The goal of MD simulations is to reproduce the time evolution of a system of N particles by solving numerically their equations of motion.[33] We rely on MD simulations to study the thermal behavior of our system through the analysis of thermal expansion, mean-square displacements, and temperature dependence of phonons. Our simulations in the hcp phase are performed at various temperatures and zero pressure by using a combination of the Nosé[34] constant-temperature and Parrinello-Rahman[35] constant-pressure techniques, this latter allowing the shape and the size of the simulation cell to vary in time. At low temperatures, the bcc phase of our model spontaneously transforms into the hcp phase when using the variable size and shape method, as shown in Ref. 24. Thermodynamical properties of the bcc phase at these temperatures can be obtained via N-V-T simulations in which the temperature is still controlled by the Nosé thermostat and the shape of the cell is kept fixed at values of the lattice parameter corresponding to the desired pressure. Under these conditions the crystal cannot transform in a perfect hcp structure. In our simulations, the fictitious mass parameter for the cell variables of the Parrinello-Rahman method is equal to $10m_{Zr}$, where m_{Zr} is the atomic mass of Zr, while the mass associated with the thermostat degree of freedom is equal to 0.1 eV ps^2. The equations of motion are integrated with use of a fifth-order Gear predictor-corrector algorithm[36] with a time step of 10^{-15} s. Periodic-boundary conditions are applied in three directions. Most simulations in the bcc phase are performed on a cubic cell containing 432 atoms. In the hcp phase, 384 atoms are arranged in a parallelepipedic cell, the axes of which are along the orthohexagonal directions. The basic orthorhombic cell defined by the [100], [120], and [001] vectors is then reproduced 6, 4, and 4 times in the three directions. A biased form of the MD algorithm is employed to relax the system upon introduction of a defect. The idea was introduced by Beeler and Kulcinsky and consists in setting to zero the velocity of a particle whenever the scalar product of its velocity and acceleration becomes negative.[37] This procedure is also known as quenched molecular dynamics.[18] When performing this calculation at constant volume, we choose the lattice parameters leading to zero pressure for the relaxed configuration.

B. The quasi-harmonic approximation

In the harmonic approximation, the full interatomic interactions are replaced by a second-order expansion of the potential energy about the ideal equilibrium lattice positions.[38] In this approximation, the lattice expansion is zero but effects of the lattice expansion on the phonon frequencies are accounted for by imposing temperature-dependent lattice parameters (the quasiharmonic approximation). In our case, the latter were determined by MD calculations, requiring zero pressure on the lattice. The phonon frequencies are then determined by diagonalization of the dynamical matrix, which is the Fourier transform of the atomic-force-constants matrices.[39] An expression of the dynamical matrix is given for the EAM potential in Ref. 15 and for the RGL potential in Ref. 40. Thermodynamical properties such as the mean-square displacement or the vibrational entropy can be computed within this approximation by sums over the phonon modes.[38] This method can also be used to determine the thermal expansion.[14]

C. Dynamical properties of phonons

The quasiharmonic approximation is valid only for infinitesimal atomic displacements. For most of the phonons this approximation remains valid even at high temperatures. However, for some particular phonons it is necessary to go beyond this second-order expansion and include anharmonic effects. This can be achieved by higher-order expansion[41,42] but the N-body character of our potential complicates dramatically these calculations. We therefore resorted to MD calculations that incorporate all anharmonic contributions. The dynamical behavior of a phonon is then revealed by the time evolution of its normal coordinate $\alpha(t)$:

$$\alpha(t)=\sum_i \mathbf{r}_i(t)\cdot\mathbf{e}_q\cos(\mathbf{q}\cdot\mathbf{l}_i)\ , \tag{17}$$

where $\mathbf{q}$ and $\mathbf{e}_q$ are the wave vector and polarization of the phonon and $\mathbf{l}_i$ and $\mathbf{r}_i$ the lattice site and atomic position of atom i. At low temperatures the normal coordinate has a sinusoidal behavior and the frequency of the phonon can be directly determined. At higher temperature this is no longer possible because of the emergence of anharmonic effects. Following Dickey and Paskin[43] we introduced a perturbation of wave vector $\mathbf{q}$, polarization $\mathbf{e}_q$, and amplitude α_0 on the atomic positions. The perturbed positions $\mathbf{r}_i'$ are related to the initial positions by

$$\mathbf{r}_i'=\mathbf{r}_i+\mathbf{e}_q\alpha_0\cos(\mathbf{q}\cdot\mathbf{l}_i)\ . \tag{18}$$

The normal coordinate is seen to oscillate with exponential decay.[43] The phonon frequency ν can be inferred from the oscillation period and the phonon lifetime τ from a fit on the exponential decay.

We applied this technique to study the behavior of the T1 N-point phonon of the bcc phase of our model. However, as it will be given in detail in Sec. IV F, the frequency of this particular mode depends on the strength of the applied perturbation. To calculate the zero-perturbation limit of the response to the displacements imposed in (18), we found it highly convenient to combine the perturbation technique of Dickey and Paskin to a procedure closely related to the subtraction technique invented by Ciccotti and Jacucci.[44] The latter method consists in measuring directly the mechanical response of a system to a suitable perturbation in the range of infinitely small applied fields. This is made possible by following simultaneously the paths of the particles in the perturbed and unperturbed trajectories and calculating the temporal variation of the response as the difference in the relevant dynamical variable. Provided that the trajectories are not too long (a few picoseconds), this procedure yields a noise-free response of the variable coupled to the external perturbation. The statistical average of this quantity is obtained by taking averages over several pairs of such perturbed and unperturbed trajectories. Since the perturbation can be infinitesimal, use of this technique does not modify the thermodynamical properties of the system. In our case, the perturbed trajectory is generated according to Eq. (18) and the dynamical variable of interest is the normal coordinate $\alpha(t)$.

IV. RESULTS

A. Monovacancy properties

The defect properties are calculated at constant zero pressure. Accordingly, the lengths of the edges of the simulation box are adjusted for both the perfect and the defective crystal to ensure zero pressure. The formation energy, E_f, and formation volume, Ω_f, of a defect are defined by comparing the properties of a system of N atoms containing one defect with those of a perfect crystal as follows:

$$E_f = N(E_d - E_0) , \tag{19}$$

$$\Omega_f = N(\Omega_d - \Omega_0) , \tag{20}$$

where E_d and E_0 are the potential energies per atom in the defective crystal and in the perfect crystal, respectively. Similar notations are used for the volumes per atom Ω_d and Ω_0.

Values of the vacancy-formation and migration energies and the vacancy-formation volume calculated with use of the $WM1$ potential are reported in Table III. Experimental results with which to compare are rather scarce. Hood[45] inferred from the absence of positron trapping at vacancies in hcp Zr an upper limit for the vacancy concentration ($c_v \approx 10^{-6}$) and then a lower limit for the formation free energy, $G_V^f = 1.35$ eV at $T = 1136$ K. It is worth mentioning that Oh and Johnson[16] have included the vacancy-formation energy in their fit of an EAM potential for hcp Zr. We feel that the experimental value they take ($E_V^f = 1.35$ eV) is underestimated, this value being the lower limit of the free energy G_V^f. From Table III one deduces a relaxation energy unusually high (25%) in the bcc phase compared with fcc (Ref. 3) (at most 3%) and other bcc elements[50] (15%). This high value and the small formation volume are evidence for a strong relaxation[51] around the vacancy and provide a viable explanation for the very weak tendency towards positrons trapping at vacancies in bcc Zr.[52] Diffusion is most likely to occur via vacancies in both hcp[45] and bcc[27,53] zirconium at least for $T \leq 0.8 T_m$, where T_m is the melting temperature. Under this assumption, values for the activation energy E_V^a can be inferred from the diffusion rate (see Table III). The agreement between the model and the available experimental data is excellent. Because of the lack of experimental data and realistic cal-

TABLE III. Defect properties in hcp and bcc zirconium. E_v^f and E_i^f are the vacancy and interstitial formation energies, E_V^m is the vacancy migration energy, E_V^a is the vacancy activation energy, and Ω_V^f and Ω_i^f are the vacancy and interstitial formation volumes. The energies are expressed in eV and the volumes are normalized to the atomic volumes $\Omega_0^{\rm hcp}$ and $\Omega_0^{\rm bcc}$. Here E_i^f refers to the most stable configurations: in the hcp phase and C configuration defined in Ref. 54 and in the bcc phase the crowdion configuration.

	hcp	bcc
Ω_V^f	0.71[a]	0.49[a]
	2.07[a]	1.53[a]
E_V^f	2.14[b]	2.10[b]
	1.55[c]	
		0.32[a]
E_V^m	0.88[a]	0.78[b]
		0.28[d]
		1.85[a]
E_V^a	2.95[a]	
		1.2–2.8[g]
	2.85[e]	
	2.46[f]	
Ω_i^f	0.84[a]	0.90[a]
E_i^f	4.27[a]	3.0[a]

[a]Calculated value for the $WM1$ potential by quenched MD.
[b]Calculated value for the $WM1$ potential prior to relaxation.
[c]Lower limit inferred from the experimental value of the free energy of Ref. 45 at 1136 K ($G_V^f > 1.35$ eV) and by assuming that $S_V^f = 2k_B$.
[d]MD result for the $WM1$ potential obtained from the vacancy jump rate (Ref. 46).
[e]The value estimated in Ref. 47 from the melting point rule (Ref. 48) for "normal" diffusion assuming a melting temperature equal to 1870 K in hcp Zr.
[f]Lower limit deduced from the experimental diffusion coefficient assuming reasonable values for the preexponential factor (as detailed in Ref. 45).
[g]Estimated from the slope of the Arrhenius plot of the experimental values of the diffusion rate (Ref. 49).

culations, our result for the vacancy-formation energy in the bcc phase is of particular interest. Further details on the properties of vacancy diffusion in bcc Zr will be given elsewhere.[25]

B. Self-interstitial properties

Self-interstitial formation energies for various configurations in the hcp phase calculated for the $WM1$ potential are listed in Table IV and compared to the values found by Oh and Johnson using an EAM potential for Zr. The notation for the self-interstitial sites is that used by Johnson and Beeler.[54] In agreement with Ref. 54, we find that the C configuration is the most stable. Self-interstitial properties in bcc structures have attracted more attention mostly because the presence of a curvature in the Arrhenius plot calls for the possible existence of a second mechanism for diffusion at high temperatures in addition to the vacancy-related one.[55] In this respect, a recent simulation study showed the spontaneous formation of Frenkel pairs in bcc Zr close to the melting point and lent support to the conjecture that interstitials may play a key role in the diffusion process.[46] Self-interstitials have been investigated experimentally in Mo and Fe and, in both cases, the favored structure is a dumbell along the [110] direction.[56] Most calculations predict the stability of a dumbell configuration in the [110] direction in Fe (Ref. 57) using a pair potential and in V, Nb, Ta,[9,18] and Mo (Ref. 9) using FS potentials. A different dumbell orientation is found for V (Ref. 22) (in the [100] direction) modeled by an EAM potential. The crowdion configuration is found in Ta, Cr,[58] and W (Refs. 18 and 58) by using FS potentials. In Table III, we list the results of our calculations of the self-interstitial formation energy and volume in Zr. The system relaxes toward the crowdion configuration, regardless of the initial configuration. The formation energy is also noteworthily low, compared with the one found in V (Ref. 22) (3.0 eV versus 4.58 eV).

On the basis of the above results for both vacancies and interstitials, we conclude that our model yields "not anomalous" defect properties in the hcp phase, low formation energies of both vacancy and interstitial, and very low vacancy-migration energy in the bcc phase. The low energies in the bcc phase are partly due to important relaxation energies.

TABLE IV. Self-interstitial formation energies in hcp Zr expressed in eV.

Configuration	Self-interstitial formation energy $WM1$	Oh and Johnson (Ref. 16)
C	4.27	4.52
B_O	4.32	4.73
O	4.48	4.62
S	Unstable, decays to C	4.92
T	Unstable, decays to C	
B_C	Unstable, decays to B_O	
B_T	Unstable, decays to B_O	Not determined

C. Thermal expansion

Thermal expansion is a crucial property to assess the reliability of our potential with respect to temperature-dependent properties. Thermal expansion of EAM-based models has been the object of recent investigations.[10,14,22] The thermal equilibrium lattice parameters are calculated for the $WM1$ potential at temperatures where the quantum effects are unimportant [the Debye temperature in hcp Zr is equal to 265 K (Ref. 29)] and zero pressure by molecular-dynamics simulations. In Fig. 2, we compare the thermal linear expansion of the model with experiment. The experimental and calculated $[\Delta a(T)]/a$ and $[\Delta c(t)]/c$ are normalized to the corresponding values at $T_{\rm ref}=293$ K in the hcp phase and $T_{\rm ref}=1200$ K in the bcc phase as follows:

$$\frac{\Delta a(T)}{a}=\frac{a(T)-a(T_{\rm ref})}{a(T_{\rm ref})} . \tag{21}$$

In the hcp phase, the lattice parameters, a and c, display a very similar behavior with increasing temperature. On the other hand, the experiments show a more pronounced

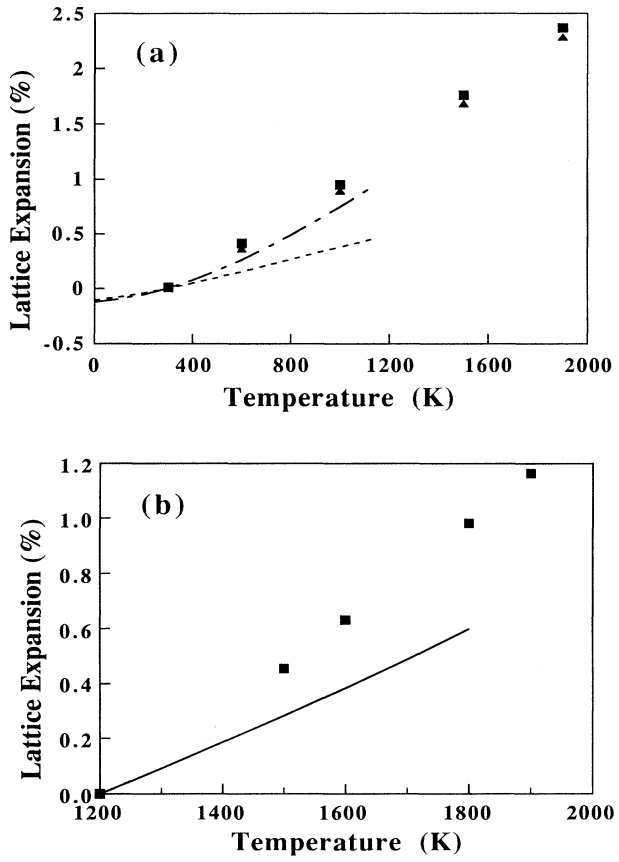

FIG. 2. Thermal linear expansion of (a) hcp and (b) bcc zirconium. The symbols are the values obtained for the $WM1$ potential from MD simulations and the lines are experimental data (Ref. 59). In (a) $\Delta a/a$ is represented by the squares and the short-dash line, and $\Delta c/c$ by the triangles and the dash-dotted line.

anisotropy. In both phases, we find an absolute value of the thermal expansion in good agreement with experiment though slightly too large. These results are quite satisfactory in view of the unphysical behavior displayed by most bcc metals modeled within the FS scheme for which thermal expansion is too small or even negative.[19] Adams and Foiles[22] suggested that this difficulty may be overcome by fitting the potentials to the full equation of state of Rose *et al.*,[60] as done for fcc metals. Along this line, an EAM potential for bcc iron has been proposed[61] but its thermal expansion has not been tested.

In our model, the volume change in the hcp-to-bcc transition is positive, as expected from the nearly ideal c/a ratio leading to a higher density in the perfectly close-packed hcp structure. On the other hand, a compression is observed experimentally; it is known as the Goldschmidt compression and seems to be related to the nonideal c/a ratio.[31] This difference, together with the fact that the fitting procedure involves the atomic volume in the hcp phase, leads to a calculated lattice parameter for the bcc phase about 1% higher than the experimental one at $T=1200$ K ($a^{\text{expt}}=0.3614$ nm,[27,59] $a^{\text{model}}=0.3652$ nm).

D. Phonon properties

Phonon-dispersion curves in α-Zr have been measured by Bezdek *et al.*[62] and then by Stassis *et al.*,[63] who emphasized, in particular, on the temperature dependence of the [001] LO-phonon frequencies. It appears indeed that the Γ[001] LO phonon has an anomalous behavior in the hcp phase of Ti, Zr, and Hf:[64] it softens appreciably with decreasing temperature and at room temperature the [001] LO branch exhibits a dip at the zone center. As expected our calculation is in excellent agreement for the small wave-vector acoustic phonons because the fitting involves the elastic constants. The major discrepancy is observed for the branches issued from the high-frequency Γ point phonon, i.e., the [001] LO, and [100] TO$\perp$, and the [110] TO$\perp$, as shown in Fig. 3(a). The anomalous experimental behavior of these branches is attributed to the detailed topology of the band structure near the Fermi energy.[64] The second-moment approximation is only sensitive to the band width and does not describe these details, therefore the RGL potentials cannot account properly for these anomalies. The same discrepancy has been observed in the case of Hf with a FS potential.[17]

Phonon-dispersion curves in β-Zr have been measured by Stassis *et al.*[65] Recently Petry *et al.*[27,66] have undertaken a systematic study of the phonon properties of three elements of group IVa, namely, Ti, Zr, and Hf. These three metals undergo the same phase transformation from the bcc to the hcp phase on lowering the temperature, and from the bcc to the ω phase under pressure. Moreover, they are characterized by the same diffusive behavior in the bcc phase. The phonon-dispersion curves of Ti, Zr, and Hf in the bcc phase display two low frequencies and strongly damped phonons at the T1 N point and L $\frac{2}{3}$[111] points. These modes are, respectively, related to the displacements promoting the two martensitic transformations mentioned above. A whole low-frequency branch connecting these two modes was found.[66] The frequency of the T1 N-point phonon has been calculated using the first-principles frozen-phonon method[67] and it turns out to be imaginary within the quasiharmonic approximation.[68] At high temperatures, substantial displacements are responsible for important anharmonic effects and the phonon-phonon coupling strength revealed by a fourth-order expansion is large enough to stabilize the T1 N-point mode.[41] The phonon-dispersion curves, calculated in the quasiharmonic approximation using the $WM1$ potential, are compared with experiments in Fig. 3(b). The overall agreement is remarkable in view of the fact that the fitting procedure deals with properties of the hcp phase only. We recall that FS potentials for bcc metals as V and Nb lead to discrepancies in the phonon-dispersion curves are as high

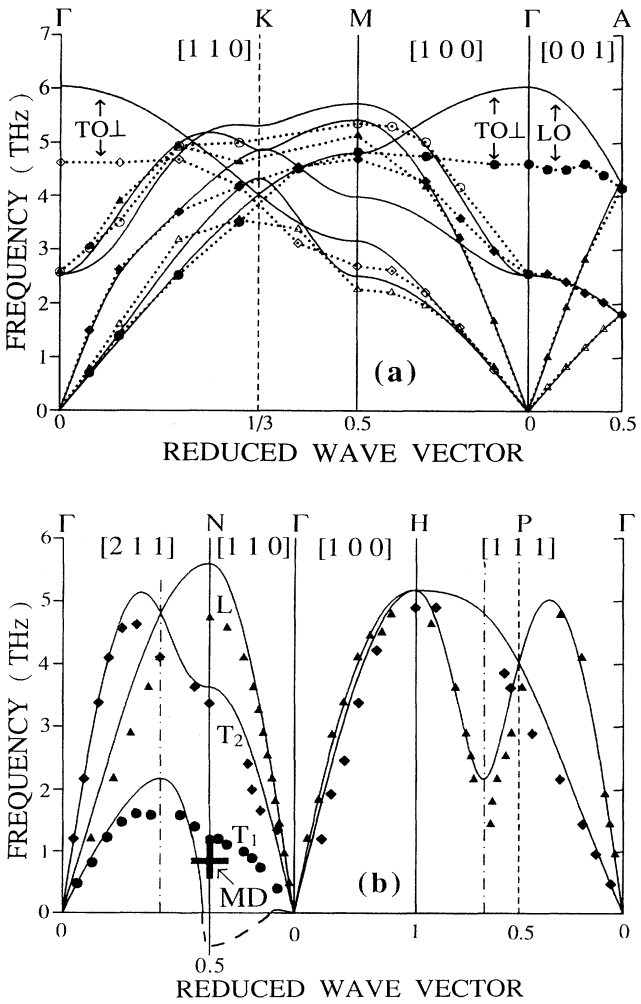

FIG. 3. Phonon-dispersion curves of (a) hcp and (b) bcc Zr. The symbols are the experimental values at 295 K (Ref. 63) in (a) and 1188 K (Ref. 66) in (b). The solid lines are the result of quasiharmonic calculations with the $WM1$ potential (the imaginary frequency branch is represented by a long-dashed line). The equivalence between the $\frac{2}{3}$[111] and $\frac{1}{3}$[211] modes is indicated by two identical vertical dash-dotted lines.

as 50%.[20] Furthermore, our potential is successful in reproducing the two relevant anomalies of bcc-Zr, namely, the low frequency of the $L\frac{2}{3}[111]$ mode and the instability of T1 N-point mode in the quasiharmonic approximation.

Figures 4(a) and 4(b) show the phonon densities of state in the hcp and the bcc phases, calculated within the quasiharmonic approximation by integration in the first Brillouin zone.[38] The result in the hcp phase is comparable to that obtained by Stassis *et al.*[63] by quasiharmonic calculations with force constants fitted to experimental dispersion curves. The discrepancy in the shape at high frequencies is related to the difference mentioned above regarding the branches issued from the high-frequency Γ point. The phonon densities of state in the bcc phase do not present any peculiarity with respect to those currently obtained for bcc structures.[38] The curves obtained for the $WM1$ and $WM2$ potentials are very similar except at low frequencies where the first singularity due to the N T1 mode in the $WM2$ plot is replaced by imaginary frequencies in the $WM1$ plot. We recall that the $WM2$ potential, resulting from a fit with a different cutoff radius (see Sec. II B), has been purposely selected because all its phonon modes are stable.

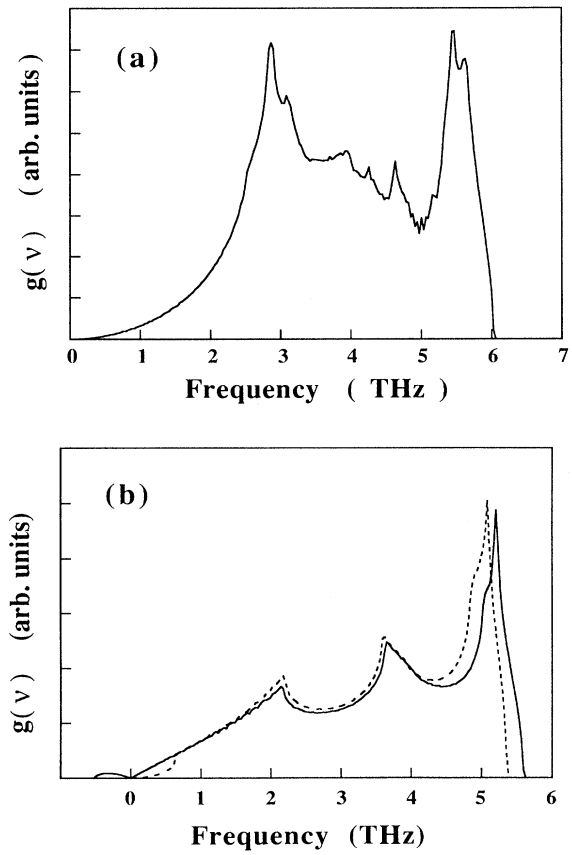

FIG. 4. The phonon density of state in (a) hcp and (b) bcc Zr calculated for the $WM1$ (solid) and $WM2$ [(dashed in (b)] potentials.

E. Temperature dependence of the T1 N-point mode

The displacement associated with the T1 N-point phonon of the bcc phase is related to the shuffle of every second (110) plane necessary to achieve the bcc- to hcp-phase transformation according to the Burgers mechanism.[24] Its wave vector $\mathbf{q}$ and polarization $\mathbf{e}_q$ are the $(\pi/a)(1,1,0)$ and $(-1,1,0)$ vectors. The experimental study of the T1 N-point phonon is highly critical because of both its low frequency (≈ 1 THz) and its very short lifetime (≈ 1.2 ps). Heiming *et al.*[66] have studied the temperature dependence of this mode by neutron-scattering measurements. According to their results, the frequency appreciably decreases as the temperature approaches the bcc-to-hcp transition temperature, but the transition occurs before it completely softens.

The dynamical behavior of the T1 N-point phonon of our model is revealed by the temporal evolution of its normal coordinate. In Fig. 5 we have represented typical signals obtained from N-V-T MD simulations at various temperatures for 10^{-11} s. At the lowest temperatures our simulations are somewhat inadequate because they do not include the quantum effects. However they are instructive to elucidate the classical behavior of our potential model with temperature. As shown in Fig. 5, at 1 K, the normal coordinate does not oscillate about zero, and its finite value reveals a finite amplitude of the shuffle of every second (110) atomic in the $[\bar{1}10]$ direction. This is the first step necessary to achieve the transition towards a close-packed structure, the second being a contraction in the [100] direction and an extension in the $[\bar{1}10]$ direction.[24] From Fig. 5 one deduces that at 1 K the phonon is unstable while at 10 K and above the phonon is stabilized. The frozen-phonon scheme helps to understand this stabilization. Following Ref. 41 we calculate the potential energy as a function of the lattice displacement corresponding to the T1 N-point mode [see Eq. (18)]. The change in energy with respect to the perfect bcc lattice is represented in Fig. 6. The negative curvature at

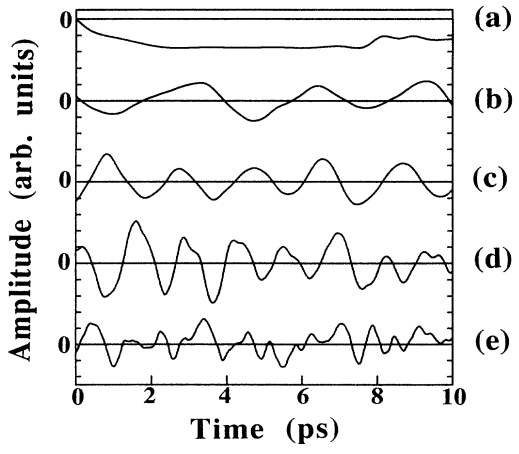

FIG. 5. Time evolution of the normal coordinate of the T1 N-point phonon at various temperatures. (a) 1 K°, (b) 10 K°, (c) 50 K°, (d) 600 K°, (e) 1200 K°.

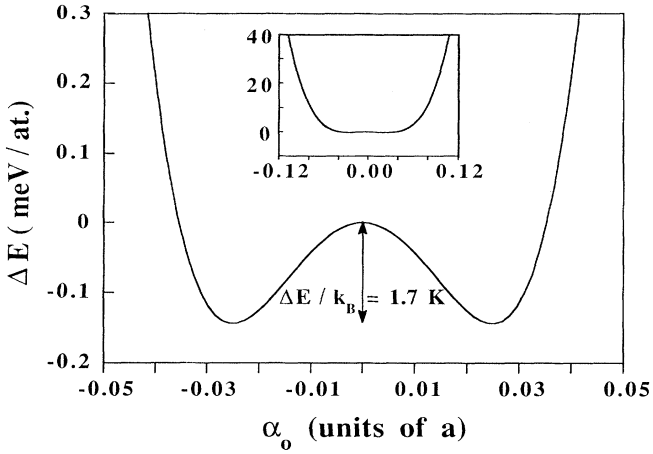

FIG. 6. Calculated potential energy as a function of the amplitude of the lattice displacement α_0 corresponding to the T1 N-point phonon in the bcc phase with the $WM1$ potential. α_0 is expressed in units of the lattice parameter a. Inset shows the same curve with different axis scales: at high temperatures the barrier becomes negligible.

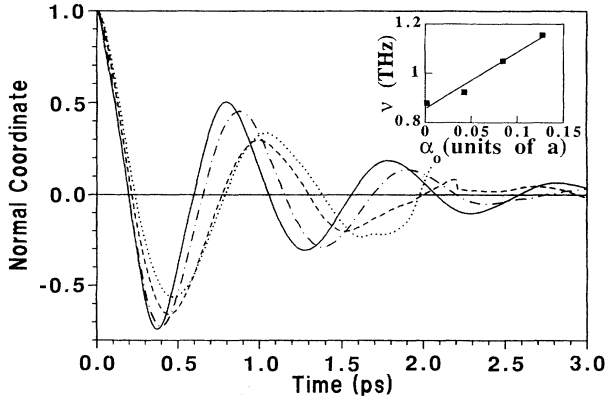

FIG. 7. Time evolution of the normal coordinate of the T1 N-point phonon at 1200 K when, initially, the atomic positions have been perturbed with various perturbation amplitudes α_0. The amplitude is normalized to the initial value. The average is taken over 20 runs for the "large" perturbations: $\alpha_0=0.042a$ (dashed), $0.085a$ (dash-dotted), and $0.13a$ (solid), where a is the lattice parameter. For the infinitesimal perturbation (dotted line), $\alpha_0=0.001a$, the average is taken over 40 runs and the procedure described in Sec. III C is used. Inset: variation of the frequency with the perturbation amplitude.

zero displacement is characteristic of the instability in the harmonic approximation. The height of the barrier between the two minima ($\Delta E/k_B=1.7$ K) gives the temperature separating the unstable and stable regimes, in excellent agreement with Fig. 5. The phonon stabilization is to be distinguished from the energetics-related stabilization of the bcc phase with respect to the hcp phase which occurs at much higher temperatures.[24] With increasing temperature, the phonon frequency increases and anharmonicity emerges. At the lowest temperatures, the phonon frequency is directly determined from Fig. 5, while at 1200 K and above the disturbance technique described in Sec. III C needs to be applied.

Dickey and Paskin showed in Ref. 43 that the frequency and the lifetime measured by the perturbation technique are independent of the perturbation amplitude, say α_0 in Eq. (18). In our case, for the T1 N-point mode, at 1200 K ($=0.56T_m$) α_0 must be as high as 10% of the lattice parameter to overcome the background noise. The perturbation is no longer small, and unlike the case reported by Dickey and Paskin, the frequency—determined from the time interval between the first and the third zero of the normal coordinate—strongly increases as α_0 increases (see Fig. 7). Indeed as α_0 increases, the anharmonic effects, which stabilize the phonon, are enhanced and the frequency rises. We thus applied the procedure described in Sec. III C to obtain a response independent of the perturbation. We employed a perturbation of amplitude α_0 equal to $0.001a$ (a being the lattice parameter) and we averaged the signal over 40 pairs of segments of 2 ps each. Such a small strength does not alter the thermodynamic properties of our system and, in particular, the anharmonic effects are not enhanced. We find that the phonon lifetime strongly decreases with temperature: From 1.2 ps at 1200 K to 0.6 ps at 1900 K. The temperature dependence of the phonon frequency is shown in Fig. 8.

We conclude that our model is successful in reproducing the harmonic instability of the T1 N-point phonon and its stabilization with temperature in agreement with the first-principles frozen-phonon calculations of Ref. 41. Moreover, the frequency of the stabilized phonon is close to the experimental value, i.e., of the order of 1 THz. On the other-hand, the frequency of our phonon is too weakly dependent on the temperature compared with both the experiments of Ref. 66 and the calculations of Ref. 41 (see Fig. 8). It is worth keeping this difference in mind

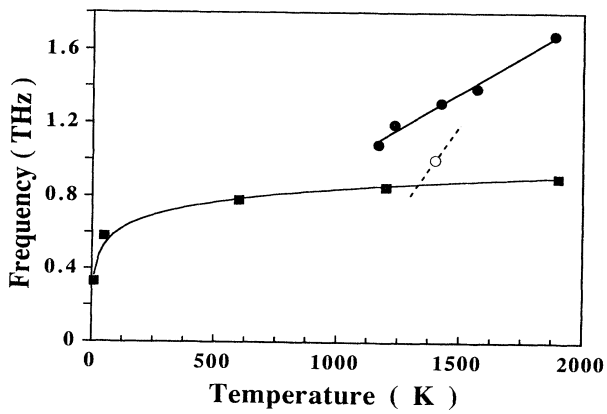

FIG. 8. Temperature dependence of the frequency of the T1 N-point phonon. The squares represent the result for the $WM1$ potential, the solid circle the experiments of Ref. 66, and the open circle the calculation of Ref. 41 (the short-dashed line indicates the predicted temperature dependence).

because the low frequencies of the mode about the T1 *N*-point contribute significantly to the mean-square displacements and the vibrational entropy.

F. Mean-square displacement

Further insight into the dynamical properties of our system can be gained by looking at the means-square displacement (MSD) defined by

$$\langle u_x^2 \rangle = \langle [x_i(t) - \bar{x}_i]^2 \rangle \ , \tag{22}$$

where $x_i(t)$ and $\bar{x}_i$ are the coordinates along the x axis of the atomic position and of the lattice site of atom i. In Eq. (22) the average is taken over several ten thousands of time steps and includes all particles. The simplest method of determining $\langle u_x^2 \rangle$ experimentally is to measure the reduction in the intensity of the elastic component of a Bragg diffraction peak produced by thermal vibrations.[69] Such experiments, to our knowledge, have not been performed on Zr. The only data available for $\langle u_x^2 \rangle$ in Zr are those calculated by Schober[70] in the quasiharmonic approximation from the experimental phonon-frequency data:[38]

$$\langle u_x^2 \rangle = \frac{\hbar}{2m} \int_0^{\omega_{\max}} \frac{g(\omega)}{\omega} \coth \left[\frac{\hbar\omega}{2k_B T} \right] d\omega \ , \tag{23}$$

where $g(\omega)$ is the phonon density of state normalized as follows:

$$\int_0^{\omega_{\max}} g(\omega) d\omega = 1 \ . \tag{24}$$

The high-temperature expansion, which is an excellent approximation for $T > T_{\text{Debye}} = 265$ K reads

$$\langle u_x^2 \rangle = \frac{k_B T}{m} \int_0^{\omega_{\max}} \frac{g(\omega)}{\omega^2} d\omega \ . \tag{25}$$

The phonon densities of state used by Schober are obtained by fitting force constants to the experimental phonon-dispersion curves at various temperatures.[27,70]

In our computations the MSD are determined by performing MD simulations and by taking into account finite-size-effect corrections.[3,40] The mean-square displacements in the hcp phase are found to be isotropic ($\langle u_x^2 \rangle \approx \langle u_y^2 \rangle \approx \langle u_z^2 \rangle$) and in excellent agreement with the calculations of Schober[70] (see Fig. 9). The MSD are larger in the bcc than in the hcp phase, thereby revealing the very different vibrational behaviors of the two phases. Our model and the calculations of Schober lead to rather different temperature dependence of the MSD in the bcc phase (see Fig. 9). When $g(\omega)$ is independent of the temperature, $\langle u_x^2(T) \rangle$ is a linear function of the temperature for $T > T_{\text{Debye}}$, as can be seen from Eq. (25). Usually one expects the phonon frequencies to be shifted toward lower values upon increasing the temperature because of the softening of the interactions due to the lattice expansion. As a consequence, $g(\omega, T_1)$ is also shifted towards lower frequencies relative to $g(\omega, T_2)$ for T_1 greater than T_2 and therefore $\langle u_x^2(T_1) \rangle$ increases relative to the value given by Eq. (25) in which $g(\omega)$ is taken to be equal to

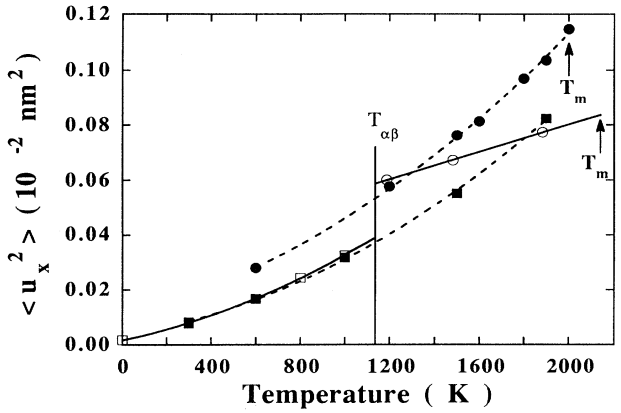

FIG. 9. Variation of the mean-square displacement as a function of temperature in hcp (square) and bcc (circle) zirconium. The values obtained for the present model (solid symbol) are compared with the quasiharmonic calculations of Schober (open symbol) (Refs. 27 and 70).

$g(\omega, T_2)$. This is indeed the case in our model in both phases. On the other hand, in the experimental case for Zr the frequencies of the modes about the T1 N point significantly increase with temperature. Because of their low values, these frequencies strongly contribute to the MSD, and lead to its decrease relative to the value obtained from Eq. (25) with $g(\omega)$ taken to be equal to $g(\omega, T = 1200$ K).

The difference between the model and the calculations of Schober on the mean-square displacement can be illustrated by their leading to different Lindemann parameters. Gilvarry[71] reformulated the Lindemann criterion for melting[72] to state that melting should occur when the root-mean-square displacement reaches a critical fraction δ of the nearest-neighbor separation d. This, known as the Lindemann law, can be written as

$$\langle u_x^2(T_m) \rangle = \delta^2 d^2 \ . \tag{26}$$

This formula has been difficult to verify because of the very few direct experimental determinations of $\langle u_x^2 \rangle$ close to the melting point, but calculations based on elastic constants data[73] or Debye temperature data[74] do suggest that the relation may be valid for crystals with similar structures. Indeed δ is of the order of 0.1 but depends on the structure, namely, $\delta_{\text{hcp}} < \delta_{\text{fcc}} < \delta_{\text{bcc}}$. The extrapolation of Schober's calculations of $\langle u_x^2 \rangle$ to the experimental melting temperature (2141 K) leads to δ equal to 0.092. In our model fusion occurred at 2000 K after a N-P-T MD run of several 10^{-10} s.[25,40] At this temperature we find for δ a value of 0.106.

V. CONCLUSIONS

N-body potentials for transition metals have been the subject of a large number of investigations in recent years. Common to most EAM or FS applications is the

use of elaborate fitting procedures developed with the intent of obtaining the best possible match between experimental and calculated quantities and based on a sometimes exceedingly high number of adjustable parameters. This paper shows that the RGL approach allows a realistic modeling of zirconium properties while conserving the intrinsic simplicity of its analytical formulation that requires only four adjustable parameters. To develop an interatomic N-body potential for zirconium, we fitted a standard, unmodified RGL form to cohesive energy, elastic constants, and equilibrium atomic volume of α-Zr. Then we checked the reliability of the potential with respect to experimental quantities other than those included in the fit, by employing various computational techniques such as static computations, quasidynamical relaxation procedures, quasiharmonic lattice-dynamics calculations, and molecular-dynamics simulations in ensembles at constant temperature and either constant volume or constant pressure.

In summary, our results are as follows. Defect properties of both the hcp and the bcc phases of Zr are consistent with the available experimental data. In particular, our results point towards low formation energies for both vacancy ($E_V^f=1.53$ eV) and interstitials ($E_i^f=3.0$ eV) (the last one being most stable in the crowdion configuration) in the β phase and low vacancy-migration energy in the β phase ($E_v^m=0.32$ eV). Our potential meets a certain degree of success with regards to thermal expansion in both phases. This is satisfactory in view of the fact that the potential was not specifically devised to obey the universal equation of state by Rose *et al.*[60] giving the total energy of the lattice under uniform compression and dilation.

Within the limitations of an inaccurate description of the details of the band structure inherent in the second-moment tight-binding approximation, we obtained phonon-dispersion curves and a phonon density of states in the hcp phase in very good agreement with experimental results. More significantly, computations of the phonon-dispersion curves in the β phase prove that the potential, fitted to properties of the α phase only, accounts properly for the instability of the T1 N-point mode in the harmonic approximation.

We paid special attention to the temperature dependence of the T1 N-point mode which promotes the bcc- to hcp-phase transformation. On the experimental side, the frequency of this phonon is seen to decrease sharply with decreasing temperature, a behavior confirmed by first-principles calculations. Our analysis of the dynamical behavior of this phonon reveals that the potential correctly models its stabilization with temperature. Less satisfactory is the weak temperature dependence of the calculated frequency of the T1 N-point mode. At high temperatures this particular frequency is obtained by perturbing the appropriate normal coordinate to overcome the coupling between modes caused by the anharmonicity. Due to the strong dependence on the applied perturbation of the calculated frequency, we proposed and tested an approach that leads to the zero-perturbation limit of the response and predicts a value of the frequency of the T1 N-point mode which is close to the experimental one at high temperatures.

Finally we focused on the comparison between our calculated mean-square displacements and the analogous quantity extracted from neutron-scattering experiments. The two sets of results agree in the hcp phase and display a marked discrepancy in the bcc phase. We were able to explain this difference in terms of the discrepancy between calculated and experimental temperature dependence of the T1 N-point mode.

The model constructed and tested in this work appears suitable for a microscopic description of both phases of Zr. We recall that recently we achieved an accurate and meaningful modeling of the dynamics of the $\beta\leftrightarrow\alpha$ transition and a sensible determination of the vibrational contribution to the excess entropy stabilizing the β phase.[24] Globally, the results we presented here, together with those concerning the mechanism and the energetics of the phase transformation, indicate that our model can be used with confidence in an attempt to clarify the high-temperature features of diffusion in β-Zr. Work along this direction, based on preliminary results contained in Ref. 46, is currently in progress.

ACKNOWLEDGMENTS

We are especially indebted to H. R. Schober for providing us with his unpublished results of the MSD calculations. During the course of this work, we benefited from highly profitable interactions with A. Heiming and W. Petry. In particular, we thank them for drawing our attention to their latest phonon measurements. We are also grateful to B. Legrand, G. Martin, and V. Pontikis for their helpful comments and suggestions. F.W. acknowledges support from the Direction des Recherches et Etudes Techniques Contract No. 87/808/20. The Laboratoire des Composés Non-Stoechiométriques is Unité associée au Centre National de la Recherche Scientifique No. 446.

[1]M. S. Daw and M. I. Baskes, Phys. Rev. B **29**, 6443 (1984).
[2]M. W. Finnis and J. E. Sinclair, Philos. Mag. A **50**, 45 (1984).
[3]V. Rosato, M. Guillopé, and B. Legrand, Philos. Mag. A **59**, 321 (1989).
[4]S. M. Foiles, M. I. Baskes, and M. S. Daw, Phys. Rev. B **33**, 7983 (1986).
[5]K. W. Jacobsen, J. K. Nørskov, and M. J. Puska, Phys. Rev. B **35**, 7423 (1987); M. S. Daw, *ibid.* **39**, 7441 (1989).
[6]J. Friedel, in *Electrons,* Vol. I of *Physics of Metals,* edited by J. M. Ziman (Pergamon, London, 1969).
[7]F. Ducastelle, J. Phys. (Paris) **31**, 1055 (1970).
[8]M. Guillopé and B. Legrand, Surf. Sci. **215**, 577 (1989).
[9]R. Rebonato, D. O. Welch, R. D. Hatcher, and J. C. Bilello, Philos. Mag. A **55**, 655 (1987).

[10]S. M. Foiles and J. B. Adams, Phys. Rev. B **40**, 5909 (1989).
[11]M. S. Daw and S. M. Foiles, Phys. Rev. Lett. **59**, 2756 (1987).
[12]B. Loisel, D. Gorse, V. Pontikis, and J. Lapujoulade, Surf. Sci. **221**, 365 (1989).
[13]J. B. Adams, S. M. Foiles, and W. G. Wolfer, J. Mater. Res. **4**, 102 (1989).
[14]S. M. Foiles and M. S. Daw, Phys. Rev. B **38**, 12 643 (1988).
[15]M. S. Daw and R. D. Hatcher, Solid State Commun. **56**, 697 (1985).
[16]D. J. Oh and R. A. Johnson, J. Mater. Res. **3**, 471 (1988).
[17]M. Igarashi, M. Khantha, and V. Vitek, in *Atomic Scale Simulation of Materials, Beyond Pair Potentials,* edited by V. Vitek and D. J. Srolovitz (Plenum, New York, 1989), p. 203.
[18]G. J. Ackland and R. Thetford, Philos. Mag. A **56**, 15 (1987).
[19]M. Marchese, G. Jacucci, and C. P. Flynn, Philos. Mag. Lett. **57**, 25 (1988).
[20]R. Rebonato and J. Q. Broughton, Philos. Mag. Lett. **55**, 225 (1987).
[21]J. Eridon and S. Rao, Philos. Mag. Lett. **59**, 31 (1989).
[22]J. B. Adams and S. M. Foiles, Phys. Rev. B **41**, 3316 (1990).
[23]U. Köhler and C. Herzig, Philos. Mag. A **58**, 769 (1988).
[24]F. Willaime and C. Massobrio, Phys. Rev. Lett. **63**, 2244 (1989).
[25]F. Willaime and C. Massobrio (unpublished).
[26]O. Fischer, M. Peter, and M. Steinemann, Helv. Phys. Acta **42**, 265 (1970).
[27]A. Heiming, Ph.D. thesis, Freie Universität Berlin, 1989; A. Heiming, W. Petry, J. Trampenau, M. Alba, C. Herzig, H. R. Schober, and G. Vogl, Phys. Rev. B **43**, 10 948 (1991).
[28]B. Legrand (unpublished).
[29]K. Masuda, N. Hamada, and K. Terakura, J. Phys. F **14**, 47 (1984).
[30]Y. Minonishi, S. Ishioka, M. Koiwa, S. Monozumi, and Y. Yamaguchi, Philos. Mag. A **43**, 1017 (1981).
[31]A. R. Kaufmann and T. T. Magel, in *Metallurgy of Zirconium,* edited by B. Lustman and F. Kerze (McGraw-Hill, New York, 1955).
[32]F. Ducastelle, Ph.D. thesis, Université de Paris–Sud, Orsay, France, 1972.
[33]For a review containing advanced applications of molecular-dynamics simulations, see G. Ciccotti and W. G. Hoover, *Molecular Dynamics Simulation of Statistical-Mechanical Systems* (North-Holland, Amsterdam, 1986).
[34]S. Nosé, J. Chem. Phys. **72**, 2384 (1984).
[35]M. Parrinello and A. Rahman, J. Appl. Phys. **52**, 7182 (1981).
[36]A. Nordsiek, Math. Comput. **16**, 22 (1962).
[37]J. R. Beeler and G. L. Kulcinski, in *Interatomic Potentials and Simulation of Lattice Defects,* edited by P. C. Gehlen, J. R. Beeler, and R. I. Jaffee (Plenum, New York, 1972), p. 735; C. H. Bennett, in *Diffusion in Solids, Recent Developments,* edited by A. S. Norwick and J. J. Burton (Academic, New York, 1975), p. 85.
[38]A. A. Maradudin, E. W. Montroll, G. H. Weis, and I. P. Ipatova, *Theory of Lattice Dynamics in the Harmonic Approximation,* 2nd ed. (Academic, New York, 1971).
[39]N. W. Ashcroft and N. D. Mermin, *Solid State Physics* (CBS, Philadelphia, 1976).
[40]F. Willaime, Ph.D. thesis, Université de Paris–Sud, Orsay, France, 1991.
[41]Y. Y. Ye, Y. Chen, K. M. Ho, B. N. Harmon, and P. A. Lindgard, Phys. Rev. Lett. **58**, 1769 (1987).
[42]R. P. Cowley, Rep. Prog. Phys. **31**, 123 (1968).
[43]J. M. Dickey and A. Paskin, Phys. Rev. **188**, 1407 (1969).
[44]G. Ciccotti and G. Jacucci, Phys. Rev. Lett. **35**, 12 (1975).
[45]G. M. Hood, J. Nucl. Mat. **96**, 372 (1981).
[46]F. Willaime and C. Massobrio, in *Atomic Scale Calculation of Structures in Materials,* edited by M. A. Schluter and M. S. Daw, MRS Symposia Proceedings No. 193 (MRS, San Francisco, CA 1990), p. 295.
[47]G. M. Hood and R. J. Schultz, Acta Met. **22**, 459 (1974).
[48]A. D. Le Claire, in *Diffusion in Body-centered Cubic Metals* (The American Society for Metals, Metals Park, OH, 1969), p. 3.
[49]G. V. Kidson, Can. J. Phys. **40**, 1563 (1963).
[50]K. Masuda, J. Phys. (Paris) **43**, 921 (1982).
[51]C. Corbel, M. Puska, and R. M. Nieminen, Rad. Effects **79**, 305 (1983).
[52]G. M. Hood, R. J. Schultz, and G. J. C. Carpenter, Phys. Rev. B **14**, 1503 (1976).
[53]C. Herzig, in *Diffusion in Materials,* edited by A. L. Laskar, J. L. Bocquet, G. Brebec, and C. Monty (Kluver Academic, Dordrecht, 1990), p. 287.
[54]R. A. Johnson and J. R. Beeler, in *Interatomic Potentials and Crystalline Defects,* edited by J. K. Lee (The Metallurgical Society of AIME, New York, 1981), p. 165.
[55]R. W. Siegel, J. N. Mundy, and L. C. Smedskjaer, Mater. Sci. Forum, **15-18**, 451 (1987).
[56]F. W. Young, J. Nucl. Mater. **69&70**, 310 (1978).
[57]R. A. Johnson, Phys. Rev. **134**, A1329 (1964).
[58]J. M. Harder and D. J. Bacon, Philos. Mag. A **54**, 651 (1986).
[59]Y. S. Touloukian, R. K. Kirby, R. E. Taylor, and P. D. Desai, in *Thermodynamical Properties of Matter* (Plenum, New York, 1975), Vol. 12, p. 400.
[60]J. H. Rose, J. R. Smith, F. Guinea, and J. Ferrante, Phys. Rev. B **29**, 2963 (1984).
[61]R. J. Harrison, A. Voter, and S. Chen, in *Atomic Scale Simulation of Materials, Beyond Pair Potentials,* edited by V. Vitek and D. J. Srolovitz (Plenum, New York, 1989), p. 219.
[62]H. F. Bezdek, R. E. Schmunk, and L. O. Finegold, Phys. Status Solidi **42**, 275 (1970).
[63]C. Stassis, J. Zarestky, D. Arch, O. D. McMasters, and B. N. Harmon, Phys. Rev. B **18**, 2632 (1978).
[64]S. H. Liu, C. Stassis, and K. M. Ho, Phys. Rev. B **24**, 5093 (1981).
[65]C. Stassis, J. Zarestky, and N. Wakabayashi, Phys. Rev. Lett. **41**, 1726 (1978); C. Stassis and J. Zarestky, Solid State Commun. **52**, 9 (1984).
[66]W. Petry, A. Heiming, J. Trampenau, M. Alba, C. Herzig, and H. R. Schober, in *Proceedings of the Third International Conference on Phonon Physics and of the Sixth International Conference on Phonon Scattering in Condensed Matter,* edited by S. Hunklinger, W. Ludwig, and G. Weis (World Scientific, Singapore, 1990), p. 1095.
[67]K. M. Ho, C. L. Fu, and B. N. Harmon, Phys. Rev. B **29**, 1575 (1984).
[68]Y. Chen, C. L. Fu, K. M. Ho, and B. N. Harmon, Phys. Rev. B **31**, 6775 (1985).
[69]C. J. Martin and D. A. O'Connor, J. Phys. C **10**, 3521 (1977).
[70]H. R. Schober (private communication).
[71]J. J. Gilvarry, Phys. Rev. **102**, 308 (1956).
[72]F. A. Lindemann, Physik. Z. **11**, 609 (1910).
[73]R. C. G. Killean and E. J. Lisher, J. Phys. C **8**, 3540 (1975).
[74]S. A. Cho, J. Phys. F **12**, 1069 (1982).